Progress In Electromagnetics Research B, Vol. 54, 69–88, 2013

ULTRAFAST ALL-OPTICAL FULL ADDER USING QUANTUM-DOT SEMICONDUCTOR OPTICAL AMPLIFIER-BASED MACH-ZEHNDER INTERFEROMETER

Mohamed Nady[1, *], Khalid F. A. Hussein[1], and Abd-El-hadi A. Ammar[2]

[1]Microwave Engineering Department, Electronics Research Institution, Cairo, Eygpt

[2]Electronics and Electrical Communications Department, Faculty of Engineering, El-AZHAR University, Cairo, Egypt

Abstract—Interferometric devices have drawn great interest in all-optical signal processing for their high-speed photonic activity. Quantum-dot semiconductor optical amplifier (QD-SOA)-based gate has added a new momentum in this field to perform all-optical logic and algebraic operations. In this paper, for the first time, a new scheme for all-optical full adder using fife QD-SOA based Mach-Zehnder interferometers is theoretically investigated and demonstrated. The proposed scheme is driven by three input data streams; two operands and a bit carried in from the next less significant stage. The proposed scheme consists of two XOR, two AND, and one OR gate. The impact of the peak data power as well as of the QD-SOAs current density, maximum modal gain, and QD-SOAs length on the ER and Q-factor of the switching outcome are explored and assessed by means of numerical simulation. The operation of the system is demonstrated with 160 Gbit/s.

1. INTRODUCTION

The demand for faster optical communication networks has been on the rise in recent years. To accommodate this demand, the new generation of optical communication networks is moving towards terabit per second data rates. Such data rates can be achieved if the data remain in the optical domain eliminating the need to convert the optical signals

Received 30 June 2013, Accepted 19 August 2013, Scheduled 27 August 2013

* Corresponding author: Mohamed Nady (mnasaed@gmail.com).

to electronic signals and back to optical signals. Therefore, to be able to achieve higher data rates successfully, advanced optical networks will require all optical ultra-fast signal processing such as wavelength conversion, optical logic and arithmetic processing, add-drop function, etc. [1–3]. All-optical combinational circuits are required for managing of the contentions and the switch control in a node of an optical packed switched network. Calculating the addition of Boolean numbers is an important functionality to perform packet header processing [4].

In recent years, optical logic gates based on several different schemes, such as dual semiconductor optical amplifier (SOA) Mach-Zehnder interferometer (MZI) [4–9], semiconductor laser amplifier (SLA) loop mirror [10, 11], ultrafast nonlinear interferometers [12, 13], and four-wave mixing process in SOA [14], are demonstrated and reported.

All-optical binary adders using many optical designs, such as terahertz optical asymmetric demultiplexers (TOADs) [15] and ultrafast nonlinear interferometers [16], have been reported. An all-optical half adder using an SOA-assisted Sagnac interferometer has been suggested and demonstrated by several groups of researchers [17–19].

A scheme for an ultrahigh-speed all-optical half adder based on four-wave mixing in SOAs has been demonstrated by Li et al. [17]. The operation of a half adder/subtractor arithmetic using the dark-bright soliton conversion control has been reported by Phongsanam et al. [18]. Menezes et al. have suggested all-optical half adder using the symmetric planar three-core non-linear directional coupler, operating with a short light pulse [19]. Finally, Scaffardi et al. have introduced all-optical full adder using a single SOA as a basic building block [4].

Among different topologies, monolithically integrated SOA-based MZI switches are the most promising candidates for all-optical signal processing devices due to their compact size, thermal stability, high-speed capability, low switching energy, relative stability, and optical integration compatibility [20–22].

The technology of quantum-dot SOAs (QD-SOAs) are very appropriate owing to its remarkably ultrafast response, which, combined with their attractive characteristics, distinguishes them from conventional SOAs [23–25]. They have larger unsaturated gain than bulk SOAs, resulting in higher power optical amplifiers, but also have enough gain at low injected currents to enable operation with low power consumption. Their saturation power can be controlled by changing the injected current with the unsaturated gain kept constant, thus enabling easy tuning of the operating point for signal amplification and processing. QD-SOAs exhibit much faster gain recovery after gain

compression than bulk SOAs, enabling amplification and processing of short pulses with negligible pulse-shape distortion. The all-optical logic gates, optical wavelength conversion, and optical regeneration based on a QD-SOA MZI are promising candidates for faster speed of operation compared with bulk and MQWSOAs due to the comparatively small electron relaxation times in QDs [26–30].

This paper introduces, for the first time (to the knowledge of the authors), a theoretical model of an ultrafast all-optical full adder based on the fife QD SOA-MZIs. The all-optical adder has potential to execute the addition in the optical domain up to 160 Gbit/s.

2. OPERATIONAL PRINCIPLE OF QD-SOA-BASED MZI

Figure 1 depicts a schematic diagram of the all-optical QD-SOA-based MZI switch. It consists of symmetrical MZI where one QD SOA is located in each arm of the interferometer [27–32]. Here, clock pulse (clk) stream composed of consecutive pulses (of wavelength λ_2) is inserted in the MZI and split via the input 3-dB coupler into a pair of equal parts, which travel separately along the identical QD-SOAs located in their path. At the same time, two input data signals (control signals), of wavelength λ_1 enter the upper and lower MZI arms, respectively, through a wavelength-selective coupler (WSC). The data pulse is at least an order of magnitude stronger than the clock pulse [31] so that only the input pulse can alter QD-SOAs optical properties. Also the detuning between the input signals and the clock pulse in the 1550-nm region is less than the homogeneous broadening of QD-SOAs 1 and 2, respectively [27–32]. In this manner, input signals can properly modify the nonlinear optical properties of the respective QD-SOAs and induce through XPM a phase difference between the two arms of the MZI. When both input data signals are 1-state or 0-state, the MZI is

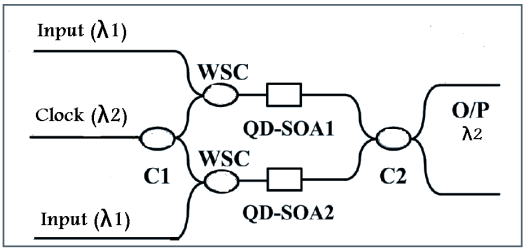

Figure 1. Schematic diagram of the all-optical QD-SOA-based MZI switch. WSC: wavelength-selective coupler; C1and C2: Couplers.

balanced, and, ideally, no pulse exits from the output port. However, when either of the input signals is in 1-state, the XPM between the input and clock pulses inside the QD-SOAs creates a differential phase shift between the two clock pulse components. When the difference is made equal to π radians, the best switching is achieved at the output port. In this present communication, we use only the output from the transmitting mode of the device which can be expressed as [27–32]

$$P_{out}(t) = \frac{P_{in}(t)}{4}\Big\{G_1(t) + G_2(t) - 2\sqrt{G_1(t) \times G_2(t)} \times \cos\left[-\frac{\alpha_{Lef}}{2}\ln\left(\frac{G_1(t)}{G_2(t)}\right)\right]\Big\} \quad (1)$$

where $P_{in}(t)$ denotes clock pulse power, $G_1(t)$ and $G_2(t)$ are the time-dependent gains experienced by the clock components in QD-SOA 1 and QD-SOA 2, respectively and α_{Lef} is the QD-SOA's linewidth enhancement factor. The time-dependent gain can be expressed as $G_{1,2}(t) = \exp(g_{1,2}(t)L_{1,2}(t))$, where $g_{1,2}(t)$ is the SOA gain and $L_{1,2}(t)$ is the active medium length. We have utilized a comprehensive model that has been widely adopted by group of scientific community for analyzing the performance of QD-SOA based MZI all-optical gates [25–32]. The photon rate equation and the associated change of the QD-SOA gain dynamics described by the three-level rate equations for the electron transitions between the wetting layer (WL), excited state (ES), and ground state (GS) are given, respectively, by [27–32]

$$\frac{\delta S}{\delta Z} = g_{\max}(2f-1)S - \alpha_{int}S \quad (2)$$

$$\frac{\delta N_\omega}{\delta t} = \frac{J}{eL_w} - \frac{N_\omega(1-h)}{\tau_{\omega 2}} + \frac{N_Q h}{L_\omega \tau_{2\omega}} - \frac{N_\omega}{\tau_{\omega R}} \quad (3)$$

$$\frac{\delta h}{\delta t} = \frac{L_\omega N_\omega(1-h)}{N_Q\tau_{\omega 2}} - \frac{h}{\tau_{2\omega}} - \frac{(1-f)h}{\tau_{21}} - \frac{f(1-h)}{\tau_{12}} \quad (4)$$

$$\frac{\delta f}{\delta t} = \frac{(1-f)h}{\tau_{21}} - \frac{f(1-h)}{\tau_{12}} - \frac{f^2}{\tau_{1R}} - \frac{g_{\max}(2f-1)L_\omega V_g}{N_Q}S \quad (5)$$

where variable Z is the longitudinal direction along the QD-SOAs length L, i.e., $Z = 0$ is for the input and $Z = L$ for the output facet of each QD-SOA, and variable t is the local time measured in a coordinate system moving with the pulse group velocity V_g. The functions used in the derivatives [Eqs. (2)–(5)] are the photon density of input data signals, which is related to their power $P(Z,t)$, with the equation as $S(Z,t) = P(Z,t)/(A_{eff}V_g h\nu)$, where $A_{eff} = 0.75\,\mu\text{m}^2$ is the effective cross section of the QD-SOAs, $V_g \approx 8.3 \times 10^7\,\text{m/s}$ is the group velocity of the propagating signal, and $h\nu$ is the photon energy

($h\nu = hc/\lambda$, where c is the speed of the light in vacuum and λ is the wavelength of the incident light). The electron density in WL is N_ω, and the electron occupation probability in the ES and GS is h and f, respectively. Also, $g = g_{\max}(2f - 1)$, where $g_{\max}$ is the maximum modal gain, α_{int} is the material absorption coefficient, J is the injection current density, e the electron charge, $\tau_{\omega 2}$ the electron relaxation time from the WL to the ES, N_Q the surface density of QDs, the L_ω effective thickness of the active layer, $\tau_{2\omega}$ the electron escape time from the ES to the WL, $\tau_{\omega R}$ the spontaneous radiative lifetime in the WL, τ_{21} the electron relaxation time from the ES to the GS, τ_{12} the electron escape time from the GS to the ES and τ_{1R} the spontaneous radiative lifetime in the QDs [27–32].

3. PRINCIPLE AND DESIGN OF PROPOSED ALL-OPTICAL FULL ADDER

A full adder adds binary numbers and accounts for values carried in as well as out. A one-bit full adder adds three one-bit numbers, often written as A, B, and C; A and B are the operands, and C is a bit carried in from the next less significant stage. The full-adder is usually a component in a cascade of adders, which add 8, 16, 32, etc. bit wide binary numbers.

As it is known, the full adder is a combinational logic circuit performing addition of three binary digits. The carry-bit is logic 1 when at least two inputs have logic 1. Otherwise, it is logic 0. The sum-bit represents the least significant bit of the three bits binary summation. The truth table shown in Fig. 2(b) explains all the expected cases for the full adder. While, Fig. 4(a) shows the concept upon which the all-

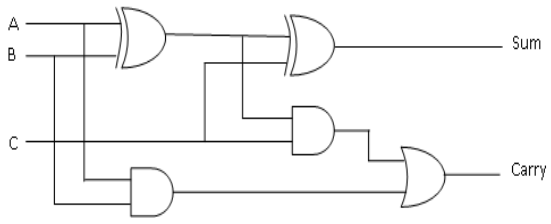

(a)

A	B	C	Sum	Carry
0	0	0	0	0
0	0	1	1	0
0	1	0	1	0
0	1	1	0	1
1	0	0	1	0
1	0	1	0	1
1	1	0	0	1
1	1	1	1	1

(b)

Figure 2. (a) Full adder logic diagram and (b) its truth table.

optical full adder circuit is designed [33]. The concept is very known. The two operands, A and B, XORed, and the output of this XOR XORed again with bit carried in from the next less significant stage to produce the SUM bit. Simultaneously, the two operands, A and B, ANDed. Then the output of the first XOR ANDed with a bit carried in from the next less significant stage. Finally, the output of the two AND gates ORed to produce the CARRY bit.

From the standpoint of optics, Fig. 3 shows the configuration of the proposed all-optical full adder. It consists of fife symmetrical QD-SOA-based MZIs (QD-SOAMZI-1 to QD-SOA MAZI-5) with the same QD-SOA placed in each of its arms. In the first and second gates (MZI-1 and MZI-2), the first XOR and first AND, respectively, the input data are A and B. On the other hand, the third and fourth gates, (MZI-3 and MZI-4), the second XOR and second AND, respectively, the input data are C and the XOR output of the MZI-1. Finally, the fifth gate,

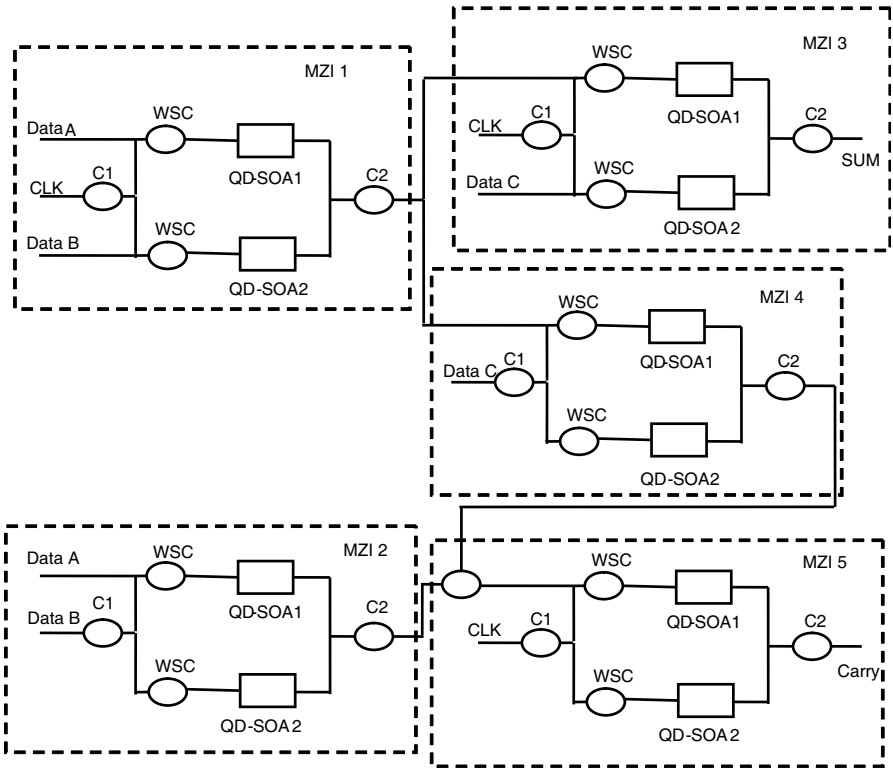

Figure 3. Configuration of the proposed all-optical full adder using fife symmetrical QD-SOAs based MZI interferometers.

OR (MZI-5), the input data are the AND outputs of the MZI-2 and MZI-4. The circuit described in Fig. 3 can be divided into three types of gates: XOR, AND, and OR gates which can be explained as follows:

Firstly, the XOR gate, the configuration of the proposed XOR gate considered in the conducted theoretical treatment, is shown in Fig. 3. It is based on the symmetrical MZI architecture, in which the same QD-SOAs, QD-SOA1 and QD-SOA2, are placed in the upper and lower arms, respectively. The first input data ($D1$) enter through a wavelength selective coupler (WSC) QD-SOA1, and the second input data ($D2$) enter through a wavelength selective coupler (WSC) QD-SOA2. The a clock stream, with the same reputation rate as the data input but a power less than the power of the data input by at least one order of magnitude, is inserted in the MZI. Then it is split via the input 3 dB coupler C1 into a pair of identical parts, which travel separately along the QD-SOAs located in their path [31]. These signals are discriminated by using different wavelengths, such that their detuning in the 1550 nm region is less than the homogeneous broadening of QD-SOA1. In this manner, the first input data $D1$ modify the nonlinear optical properties of QD-SOA1 and induce a change on the gain and phase of the upper part of the clock stream, and the second input data $D2$ do the same thing on the lower part of the clock stream. Now if both $D1$ and $D2$ equal '0' or '1' then QD-SOA1 remains intact to the same dynamical state as QD-SOA2 so that the decomposed constituents of the clock stream perceive the same gain. Thus when they recombine at 3 dB coupler C2, they interfere destructively, which results in a space or pulse free at output port. On the other hand, if one of $D1$ or $D2$ equals '1' and the other equals '0' then one of QD-SOA1 or QD-SOA2 undergoes a radical change of its gain compared to the non-driven QD-SOA (which has input equal to '0'). Consequently, the copy of the clock stream in one MZI arm acquires via cross-phase modulation [27] a nonlinear phase shift against its counterpart in the other MZI arm, which eventually creates a relative phase difference between these components. If this quantity is ideally made equal to π then it is possible to maximize the amount of the power that emerges at output port and hence the amplitude of the obtained logic one. According to this mode of operation a pulse occurs at output port if and only if a pulse is present in only one input data ($D1$ or $D2$) whilst no pulse appears at the specific terminal if $D1$ and $D2$ are similar.

It should be noted that $D1$ in the above description represents data A for the first XOR (MZI 1), whilst it represents the first XOR output for the second XOR (MZI 3). On the other hand, $D2$ in the above description represents data B for the first XOR (MZI 1), whilst it represents data C for the second XOR (MZI 3).

Secondly, the AND gate, the configuration of the proposed AND gate considered in the conducted theoretical treatment, is shown in Fig. 3. It is based on the symmetrical MZI architecture, in which the same QD-SOAs; QD-SOA1 and QD-SOA2, are placed in the upper and lower arm, respectively. The first input data ($D3$) enter through a wavelength selective coupler (WSC) QD-SOA1, while the second input data ($D4$) are inserted in the MZI and split via the input 3 dB coupler C1 into a pair of identical parts, which travel separately along the QD-SOAs located on their path. The first input data should be at least an order of magnitude stronger than the second input data [34]. These signals are discriminated by using different wavelengths, such that their detuning in the 1550 nm region is less than the homogeneous broadening of QD-SOA1. In this manner, only the first input data can modify the nonlinear optical properties of QD-SOA1 and induce a change on the gain and phase of the second input data. Now if $D4$ = '0' then regardless of the binary content of $D3$ we get nothing at output port, simply because there is no input signal on which to imprint any perturbation of the initially balanced MZI and to transfer to the output port. This is a trivial situation, which changes when $D4$ = '1', namely when data sequence $D4$ contains a pulse. In this case the result at output port depends on the existence of a pulse in the same bit slot of data sequence $D3$. More specially, if $D3$ = '0', QD-SOA1 remains intact at the same dynamical state as QD-SOA2 so that the decomposed constituents of $D4$ perceive the same gain. Thus when they recombine at 3 dB coupler C2, they interfere destructively, which results in a space pulse free at output port. But if $D3$ = '1' QD-SOA1 undergoes a radical change of its gain compared to the non-driven QD-SOA2. Consequently, the copy of $D4$ in the upper MZI arm acquires via cross-phase modulation [34] a nonlinear phase shift against its counterpart in the lower MZI arm, which eventually creates a relative phase difference between these components. If this quantity is ideally made equal to π, then it is possible to maximize the amount of the power that emerges at output port and hence the amplitude of the obtained logic one. According to this mode of operation, a pulse occurs at output port, if and only if a pulse is present in both input data ($D3$ and $D4$) whilst no pulse appears at the specific terminal if a pulse is absent from either $D3$ or $D4$ or from both of them.

It should be noted that $D3$ in the above description represents data A for the first AND (MZI 2), whilst it represents the first XOR output for the second AND (MZI 4). On the other hand, $D4$ in the above description represent data B for the first AND (MZI 2), whilst it represents data C for the second AND (MZI 4).

Finally, the OR gate, the configuration of the proposed OR gate

considered in the conducted theoretical treatment, is shown in Fig. 3. It is based on the symmetrical MZI architecture, in which the same QD-SOAs; QD-SOA1 and QD-SOA2, are placed on the upper and lower arms, respectively. The input data (D) enter through a wavelength selective coupler (WSC) QD-SOA1, these input data consist of the two output data of the two AND gates (MZI 2, MZI 4), combined through a wavelength selective coupler (WSC). While a clock stream with the same reputation rate as the data input but a power less than the power of the data input by at least one order of magnitude is inserted in the MZI and is split via the input 3 dB coupler C1 into a pair of identical parts, which travel separated along the QD-SOAs located in their path [35]. These signals are discriminated by using different wavelengths, such that their detuning in the 1550 nm region is less than the homogeneous broadening of QD-SOA1. In this manner, only the input data (D) can modify the nonlinear optical properties of QD-SOA1 and induce a change on the gain and phase of the clock stream. Now if $D =$ '0' which means the two output of the two AND gates equal to zero, then QD-SOA1 remains intact to the same dynamical state as QD-SOA2 so that the decomposed constituents of the clock stream perceive the same gain. Thus when they recombine at 3 dB coupler C2, they interfere destructively, which results in a space or pulse free at output port. The output equals zero. But if $D =$ '1' which means that at least one of the two AND gate outputs equals one, QD-SOA1 undergoes a radical change of its gain compared to the non-driven QD-SOA2. Consequently, the copy of clock stream in the upper MZI arm acquires via cross-phase modulation [35] a nonlinear phase shift against its counterpart in the lower MZI arm, which eventually creates a relative phase difference between these components. If this quantity is ideally made equal to π, then it is possible to maximize the amount of the power that emerges at output port and hence the amplitude of the obtained logic one. According to this mode of operation, a pulse occurs at output port of the OR gate if and only if a pulse is present at any of the outputs of the two AND gates (MZI 2, MZI 4) whilst no pulse appears at the specific terminal if a pulse is absent from both MZI 1 output and MZI 2 output.

It has to be noted that the output of any gate has to be attenuated before using it as input to the next gate to avoid the cascading amplification.

4. SIMULATION RESULTS OF THE ALL-OPTICAL FULL ADDER

In order to study the performance of the proposed QD-SOA based MZI, we have solved the coupled Eqs. (2)–(5) numerically in a step wise manner for pulses of input data A, B, and C that belong to a 160 Gbit/s pseudo-random binary sequence and have a Gaussian power profile [30]:

$$P_\gamma(0,t) = P_{\max} \exp\left(-\frac{4Ln(2)(t-0.5*BD)^2}{PW^2}\right), \quad \gamma = A,B,C \quad (6)$$

where $P_{\max}$ is their peak power, and $PW = 2\,\text{ps}$ is their full width at half maximum. $BD = 6.25\,\text{ps}$ is the bit duration. Then the 4th order Runge-Kutta method is applied to find the amplification factors in both MZI arms, which are expressed by

$$G_1 = S_{upper}(L,t)/S_{upper}(0,t) \quad (7)$$

$$G_2 = S_{Lower}(L,t)/S_{Lower}(0,t) \quad (8)$$

In this QD-SOA model, the values of the different parameters are taken from the literature on other QD-SOA based interferometric gates [27–34].

All parameters used in the calculations are summarized in Table 1.

Table 1. Parameters used for simulation of the all-optical full adder.

Parameter	Value	Parameter	Value
$g_{\max}$	$14\,\text{cm}^{-1}$	τ_{21}	0.16 ps
α_{int}	$2\,\text{cm}^{-1}$	τ_{12}	1.2 ps
τ_{GS}^{spon}	1200 ps	τ_{1R}	0.4 ns
τ_{w2}	3 ps	$P_{\max}$	11dBm
N_Q	$5 \times 10^{10}\,\text{cm}^{-2}$	L	4 mm
L_w	0.25 μm	J	$4\,\text{kA/cm}^2$
τ_{2w}	1 ns	α_{Lef}	4.5
τ_{WR}	0.2 ns		

In order to assess the performance of the full adder circuit at 160 Gbit/s, we have to chose which output (Carry or SUM)) we will study and what is the suitable metric for this purpose.

We will study the Carry bit because it deals with a higher number of gats (4 gates) than the SUM bit (2 gates). With respect to chosing the suitable metric, this can be done with the help of the truth table of the full adder shown in Fig. 2(b). More specifically, we observe

that of the eight logical possibilities, marks (1) and spaces (0) are equal (4 times for each case). Therefore, we must focus on how to distinguish marks from the spaces. Hence, the most suitable metric for this purpose is the extinction ratio and the Quality factor [36].

Figure 4 illustrates the effect on the ER with peak power of the input data signals for three different current density values, when the other parameters are kept fixed. The common characteristic of all curves is that the ER is increased with power up to a certain value after that it is decreased. The maximum value changes and shifts to the right as the current density becomes larger. From a physical perspective this happens because the current density determines the power required to alter the optical properties of a QD-SOA and properly saturate its gain, and the higher it is, the more power is necessary for this purpose [37]. This fact also explains that as we move well enough into the falling slope of the curves, a larger current density is necessary to enhance the ER and hence improve performance for a given power. This in turn allows selecting the peak data power from a wider range of permissible values, which potentially offers greater flexibility in the design of the full adder circuit.

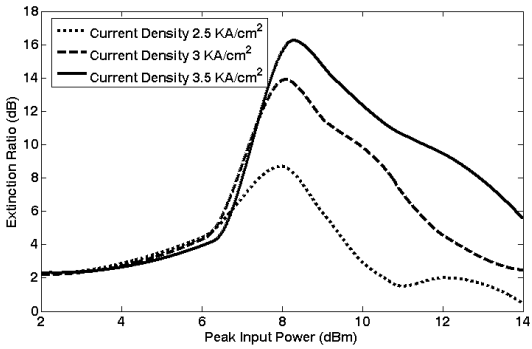

Figure 4. Variation of extinction ratio (ER) with peak data power for different current densities, keeping other parameters fixed.

Figure 5 shows the variation of ER with QD-SOAs length for three different peak control powers. The common characteristic of all curves is that the ER is increased with QD-SOAs length to a certain value after that it is dropped. The maximum value is shifted to the left as the peak power becomes larger. Smaller value of the QD-SOA length requires larger peak control power to obtain the maximum value of ER. Thus from Figs. 4 and 5, we say that larger current density and longer QD-SOAs length are preferable for obtaining a satisfactory performance in terms of the ER with reduced control power lying in a

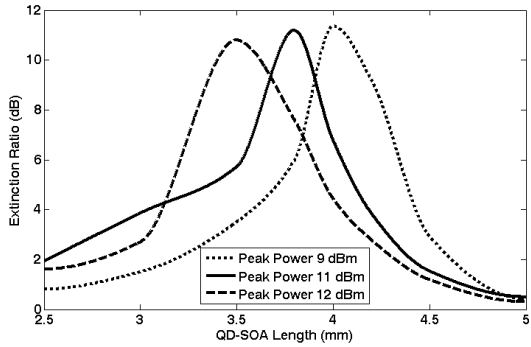

Figure 5. Variation of extinction ratio (ER) with QD-SOA length for different peak data power, keeping other parameters fixed.

wider span. In reality, however, this choice is technically limited by the fact that the extra bias current, which is required either for providing a higher current density in a given QD-SOA device or achieving the same current density in a longer QD-SOA, might not be reasonable for practical QD-SOAs [37, 38].

Figure 6 shows the variation of ER with current densities for three different QD-SOA lengths. From this figure, it is observed that among the three QD-SOAs lengths the ER becomes acceptable only for 3.5 and 4 mm. This in turn allows keeping the current density below 4 kA/cm, since after reaching its defined minimum, the ER becomes almost independent of this parameter because there is an oversupply of carriers and because the QD-SOA is sufficiently biased to the desired point.

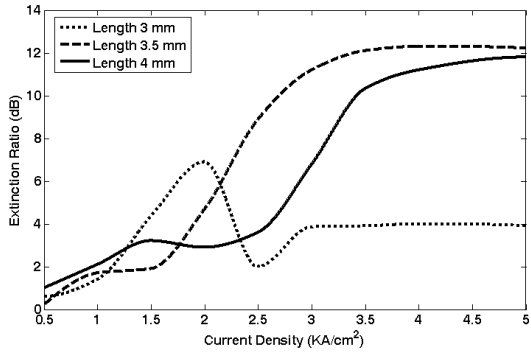

Figure 6. Variation of ER with current densities for three different QD-SOAs length, keeping other parameters fixed.

Figure 7 shows the variation of ER with the maximum modal gain for three different QD-SOAs lengths. The common characteristic of all curves is that the ER is increased with the maximum modal gain to a certain value after that it is dropped. The maximum value is shifted to the right as the QD-SOAs length becomes smaller. The smaller value of the maximum modal gain requires longer QD-SOAs length to obtain the maximum value of ER.

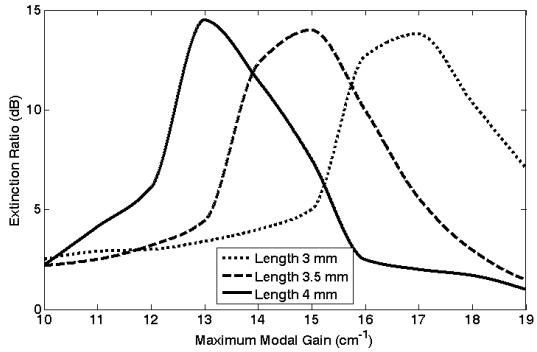

Figure 7. Variation of ER with the maximum modal gain for three different QD-SOAs length, keeping other parameters fixed.

Figure 8 shows that the ER is very sensitive to the variations of the electron relaxation time from the ES (excited state) to the GS (ground state) since the slope of the curve is decreased in an exponential-like manner as this relaxation time is increased, finally becoming smoother near the left edge of the diagram. So the transition time between ES and GS must be kept below some value and ideally as fast as possible. In this curve, it has to be below 0.25 ps to obtain ER a round 10 dB.

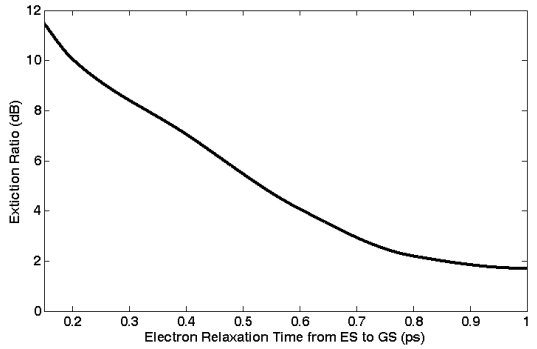

Figure 8. Variation of ER with electron relaxation time from the ES to the GS.

Figure 9 illustrates the effect on the Q-factor with current densities for three different maximum modal gains, when the other parameters are kept constant. The common characteristic of all curves is that the Q-factor is increased with current density up to a certain value after that it is decreased. The maximum value of Q-factor is dropped when the value of $g_{\max}$ is outside a certain range. So the value of $g_{\max}$ must be fixed at a particular value to achieve the maximum Q-factor value.

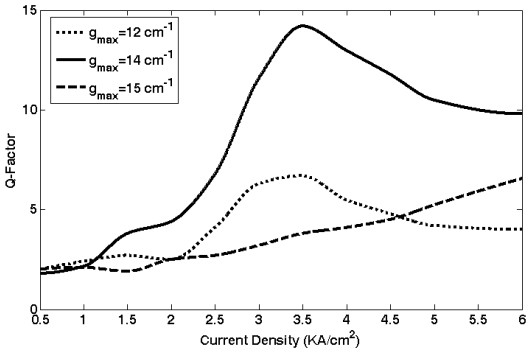

Figure 9. Variation of Q-factor with current densities for three different maximum modal gains, when the other parameters are kept constant.

Figure 10 shows the variation of Q-factor with current densities for three different QD-SOA lengths. From this figure, it is observed that among the three QD-SOA lengths, the Q-factor becomes acceptable only for 4 mm. Thus from Figs. 9 and 10, we say that increasing injection current up to a value approximately 3.5 kA/cm, more carriers

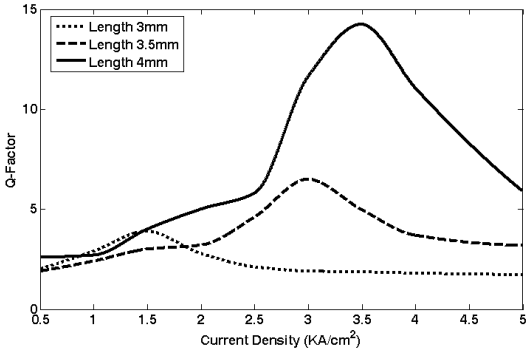

Figure 10. Variation of Q-factor with current densities for three different QD-SOAs length, when the other parameters are kept fixed.

are injected to the wetting layer. Thus each energy level in the QD can recover to its initial carrier density faster after carrier depletion by the injected pulse. So, up to a certain value approximately 3.5 kA/cm of the injection current, the Q-factor value increases. After a value (approximately above 3.5 kA/cm) of the injection current, more carriers in the conduction band will be depleted due to stimulated emission. So the QD energy states will take much longer time to recover their carrier density level, hence decrease the output quality.

According thus to Figs. 4–10 and their interpretation, it can be inferred that the requirements for the critical parameters are $8\,\text{dBm} \leq P_{\max} \leq 11\,\text{dBm}$, $3.5\,\text{kA/cm}^2 \leq J \leq 4.5\,\text{kA/cm}^2$, $3.7\,\text{mm} \leq L \leq 4.2\,\text{mm}$, $13.5/\text{cm} \leq g_{\max} \leq 14.5/\text{cm}$ and $0.15\,\text{ps} \leq \tau_{21} \leq 0.3\,\text{ps}$. By following these guidelines and using the combination of values $P_{\max} = 10.5\,\text{dBm}$, $J = 4\,\text{kA/cm}^2$, $L = 4\,\text{mm}$, $g_{\max} = 14/\text{cm}$, and $\tau_{21} = 0.16\,\text{ps}$, respectively, which obviously is not unique and falls within the specified boundaries. A more than adequate Q-factor about 12.5 dB and ER about 11.7 dB can be obtained, which is reflected on the high quality of pulse stream obtained at the output [36]. The input waveforms and simulated output waveforms are shown in Figs. 11(a)–(e), respectively. The eye-diagram is the superposition of the outputs for the repetition period of the inputs. Fig. 12 is not a classical eye-diagram because it is not as informative in the sense that degrading effects, normally observed in the point-to-point communication links [36], such as noise

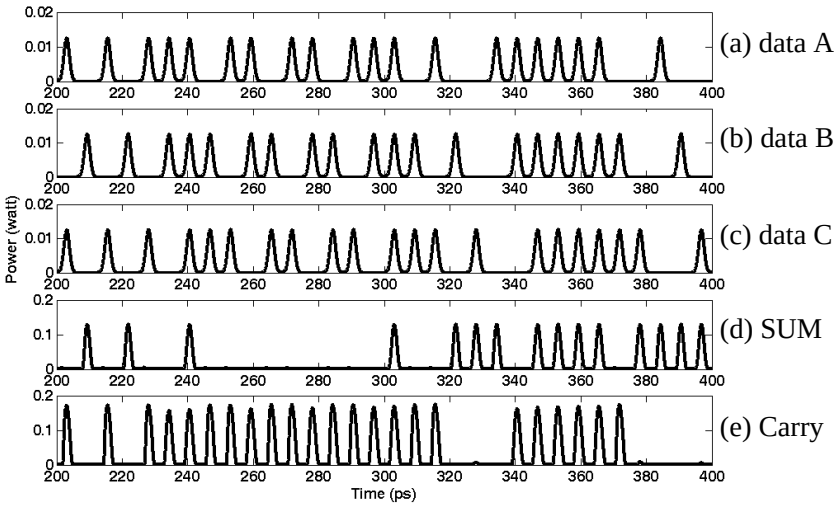

Figure 11. Waveforms of all-optical full adder, where (a) input data stream A, (b) input data stream B, (c) input data stream C (C_{in}), (d) output sum-bit (S) and (e) output carry-bit (C_{out}).

source, are added by the detector and optical fibers. This diagram is called a pseudo-eye-diagram [39]. The relative eye opening (O) is defined as $O = (P^1_{\min} - P^0_{\max})/P^1_{\min}$, where $P^1_{\min}$ and $P^0_{\max}$ are the minimum and maximum powers at 1-state and 0-state, respectively. An eye-diagram with large eyes indicates a clear transmission with a low bit rate. Here, we get PED $O = 92\%$. This value indicates a quite good response of the circuit under consideration at its output terminals. The cascadeability refers to the ability of a switch to drive directly from its main output to another input where the signal responsible for switching is launched and constitutes a key requirement for the perspective of building combinational circuits. In the cascading stages, the extinction ratio will be decreased and Q-factor value maybe increased at the output. In the cascading circuit, high input power at the previous stages is required to provide sufficient pump power at the input of the subsequent cascading stages. This high pump power degrades the extinction ratio at the subsequent stages of the subsystem. Moreover, it leads to improvement of the output Q-factor value, and the power transfer function of the QD-SOA becomes steeper due to the deep gain saturation caused by the incoming pulses in cross gain modulation operation. It is also noted that the performance of the subsequent system, which is limited by the degradation of the extinction ratio, is expected to be significantly enhanced using saturable absorbers [40].

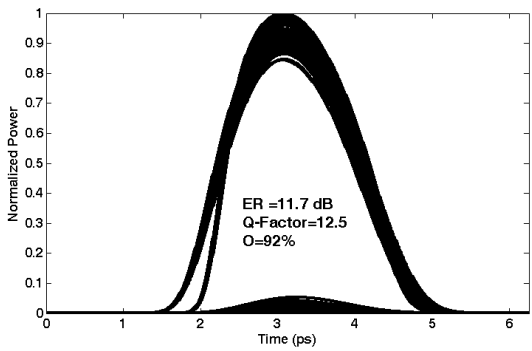

Figure 12. Simulated output waveforms with pseudo-eye-diagram (PED).

5. CONCLUSIONS

The feasibility of realizing an ultrafast all-optical full adder using fife QD-SOA based Mach-Zehnder interferometers is theoretically investigated and demonstrated. Numerically simulated results

confirming the described method is also given in this paper. The impact of the peak data power as well as of the QD-SOAs current density, maximum modal gain, and QD-SOAs length on the ER and Q-factor at the output has been thoroughly investigated. The performance of this optical circuit is extremely fast, and operation of the system is demonstrated with 160 Gbit/s. It is important to note that the predetermined values of the intensities of laser light for incoming pluses and input data signals are needed to send optical signal in desired channels. In our proposed design, the measured values of ER and Q-factor are about 11.7 dB and 12.5, respectively, which are adequate for all-optical logic based information processing systems. This circuit can be used to design many complex all-optical circuits. The model can be extended for studying more complex all-optical circuits of enhanced functionality in which the proposed circuit developed in this paper may be assumed as the basic building blocks.

REFERENCES

1. Roy, J. N., "Mach-Zehnder interferometer-based tree architecture for all-optical logic and arithmetic operations," *Optik*, Vol. 120, 318–324, 2009.
2. Garg, A. K. and R. S. Kaler, "Novel optical burst switching architecture for high speed networks," *Chinese Optics Letters*, Vol. 6, No. 11, 807–811, 2008.
3. Stubkjaer, K. E., "Semiconductor optical amplifier-based all-optical gates for high-speed optical processing," *IEEE J. Sel. Topics Quantum Electron.*, Vol. 6, 1428–1435, 2000.
4. Scaffardi, M., P. Ghelfi, E. Lazzeri, L. Poti, and A. Bogoni, "Photonic processing for digital comparison and full addition based on semiconductor optical amplifiers," *IEEE Journal of Quantum Electronics*, Vol. 14, No. 3, 826–832, 2008.
5. Wang, Q., G. Zhu, H. Chen, J. Jaques, J. Leuthold, A. B. Piccirilli, and N. K. Dutta, "Study of all-optical XOR using Mach-Zehnder interferometer and differential scheme," *IEEE Journal of Quantum Electronics*, Vol. 40, No. 6, 703–710, Jun. 2004.
6. Clavero, R., F. Ramos, J. M. Martinez, and J. Marti, "All-optical flip-flop based on a single SOA-MZI," *IEEE Photonics Technology Letters*, Vol. 17, No. 4, 843–845, 2005.
7. Kim, J. Y., J. M. Kang, T. Y. Kim, and S. K. Han, "10 Gbit/s all-optical composite logic gates with XOR, NOR, OR and NAND functions using SOA-MZI structures," *Electron. Lett.*, Vol. 42, 303, 2006.

8. Ye, X., P. Ye, and M. Zhang, "All-optical NAND gate using integrated SOA-based Mach-Zehnder interferometer," *Opt. Fiber Technol.*, Vol. 12, 312–316, 2006.
9. Minh, H. L., F. Z. Ghassemlooy, and W. P. Ng, "All-optical flip-flop based on a symmetric Mach-Zehnder switch with a feedback loop and multiple forward set/reset signals," *Opt. Eng.*, Vol. 46, No. 4, 40501-03, 2007.
10. Hong, W., D. Huang, and G. Zhu, "Switching window of an SOA loop mirror with SOA sped-up by a CW assist light at transparency wavelength," *Opt. Commun.*, Vol. 238, Nos. 1–3, 151–156, 2004.
11. Roy, J. N. and D. K. Gayen, "Integrated all-optical logic and arithmetic operations with the help of TOAD based interferometer device-alternative approach," *Appl. Opt.*, Vol. 46, No. 22, 5304–5310, 2007.
12. Li, D., X. Zhang, and D. Huang, "Novel all-optical format conversion using an ultrafast nonlinear interferometer at 10–40 Gbit/s," *Microw. Opt. Technol. Lett.*, Vol. 49, No. 3, 508–510, 2007.
13. Zoiros, K. E., P. Avramidis, and C. S. Koukourlis, "Performance investigation of semiconductor optical amplifier based ultrafast nonlinear interferometer in nontrivial switching mode," *Opt. Eng.*, Vol. 47, No. 11, 115006-11, 2008.
14. Han, L., H. Wen, H. Zhang, and Y. Guo, "All-optical wavelength conversion for polarization shift keying signal based on four-wave mixing in a semiconductor optical amplifier," *Opt. Eng.*, Vol. 46, No. 9, 090501-3, 2007.
15. Chen, Z., "Simple novel all-optical half adder," *Opt. Eng.*, Vol. 49, No. 4, 043201-6, 2010.
16. Tsiokos, D., E. Kehayas, K. Vyrsokinos, T. Houbavlis, L. Stampoulidis, G. T. Kanellos, N. Pleros, G. Guekos, and H. Avramopoulos, "10-Gb/s all-optical half adder with interferometric SOA gates," *IEEE Photon. Technol. Lett.*, Vol. 16, No. 3, 284–286, Mar. 2004.
17. Li, P.-L., D.-X. Huang, X.-L. Zhang, and G.-X. Zhu, "Ultrahigh speed all-optical half adder based on four-wave mixing in semiconductor optical amplifier," *Optics Express*, Vol. 14, No. 24, 11839–11847, 2006.
18. Phongsanam, P., S. Mitatha, C. Teeka, and P. P. Yupapin, "All optical half adder/subtractor using dark-bright soliton conversion control," *Microw. Opt. Technol. Lett.*, Vol. 53, No. 7, 1541–1544, 2011.

19. Menezes, J. W. M., W. B. Fraga, A. C. Ferreira, G. F. Guimaraes, A. F. G. F. Filho, C. S. Sobrinho, and A. S. B. Sombra, "All-optical half adder using all-optical XOR and AND gates for optical generation of "Sum" and "Carry"," *Fiber Integr. Opt.*, Vol. 29, No. 4, 254–271, 2010.
20. Nakamura, S., Y. Ueno, K. Tajima, J. Sasaki, T. Sugimoto, T. Kato, T. Shimoda, M. Itoh, H. Hatakeyama, T. Tamanuki, and T. Sasaki, "Demultiplexing of 168-Gb/s data pulseswith a hybrid-integrated symmetric Mach-Zehnder all-optical switch," *IEEE Photon. Technol. Lett.*, Vol. 12, No. 5, 425–427, May 2000.
21. Kim, J. Y., J. M. Kang, T. Y. Kim, and S. K. Han, "All-optical multiple logic gates with XOR, NOR, OR, and NAND functions using parallel SOA-MZI structures: Theory and experiment," *J. Lightw. Technol.*, Vol. 24, No. 9, 3392–3399, Sep. 2006.
22. Berg, T. W. and J. Mork, "Saturation and noise properties of quantum-dot optical amplifiers," *IEEE Journal of Quantum Electronics*, Vol. 40, No. 11, 1527–1539, Nov. 2004.
23. Li, X. and G. Li, "Comments on 'Theoretical analysis of gain recovery time and chirp in QD-SOA'," *IEEE Photon. Technol. Lett.*, Vol. 18, No. 22, 2434–2435, Nov. 2006.
24. Ben-Ezra, Y., B. I. Lembrikov, and M. Haridim, "Acceleration of gain recovery and dynamics of electrons in QD-SOA," *IEEE Journal of Quantum Electronics*, Vol. 41, No. 10, 1268–1273, 2005.
25. Ben-Ezra, Y., M. Haridim, and B. I. Lembrikov, "Theoritical analysis of gain-recovery time and chirp in QD-SOA," *IEEE Photon. Technol. Lett.*, Vol. 17, No. 9, 1803–1805, Sep. 2005.
26. Rostami, A., H. B. A. Nejad, R. M. Qartavol, and H. R. Saghai, "Tb/s optical logic gates based on quantum-dot semiconductor optical amplifiers," *IEEE Journal of Quantum Electronics*, Vol. 46, No. 3, 354–360, Mar. 2010.
27. Ben-Ezra, Y., B. I. Lembrikov, and M. Haridim, "Ultrafast all-optical processor based on quantum-dot semiconductor optical amplifiers," *IEEE Journal of Quantum Electronics*, Vol. 45, No. 1, 34–41, Jan. 2009.
28. Dimitriadou, E. and K. E. Zoiros, "On the feasibility of ultrafast all-optical NAND gate using single quantum-dot semiconductor optical amplifier-based Mach-Zehnder interferometer," *Opt. Laser Technol.*, Vol. 44, No. 6, 1971–1981, 2012.
29. Dimitriadou, E. and K. E. Zoiros, "Proposal for all-optical NOR gate using single quantum-dot semiconductor optical amplifier-based Mach-Zehnder interferometer," *Opt. Commun.*, Vol. 285, 1710–1716, 2012.

30. Dimitriadou, E. and K. E. Zoiros, "On the design of ultrafast all-optical NOT gate using quantum-dot semiconductor optical amplifier-based Mach-Zehnder interferometer," *Opt. Laser Technol.*, Vol. 44, 600–607, 2012.
31. Han, H., M. Zhang, P. Ye, and F. Zhang, "Parameter design and performance analysis of an ultrafast all-optical XOR gate based on quantum-dot semiconductor optical amplifiers in nonlinear Mach-Zehnder interferometer," *Opt. Commun.*, Vol. 281, 5140–5145, 2008.
32. Rostami, A., H. B. A. Nejad, R. M. Qartavol, and H. R. Saghai, "Tb/s optical logic gates based on quantum-dot semiconductor optical amplifiers," *IEEE Journal of Quantum Electronics*, Vol. 46, No. 3, 354–360, Mar. 2010.
33. Morris Mano, M., *Digital Logic and Computer Design*, 119–123, Prentice-Hall, 1979, ISBN 0-13-21450-3.
34. Dimitriadou, E. and K. E. Zoiros, "On the feasibility of 320 Gb/s all-optical and gate using quantum-dot semiconductor optical amplifier-based Mach-Zehnder interferometer," *Progress In Electromagnetics Research B*, Vol. 50, 113–140, 2013.
35. Rostami, A. and H. Baghban, *Nanostructure Semiconductor Optical Amplifiers: Building Blocks for All-optical Processing*, Springer, 2011.
36. Agrawal, G. P., *Fiber-optic Communication Systems*, Wiley, New York, 2002.
37. Yang, W., M. Zhang, and P. Ye, "Analysis of all-optical demultiplexing from 160/320 Gbit/s to 40 Gbit/s using quantum-dot semiconductor optical amplifiers assisted Mach-Zehnder interferometer," *Microw. Opt. Technol. Lett.*, Vol. 52, 1629–1633, 2010.
38. Pina, J. F., H. J. A. da Silva, P. N. Monteiro, J. Wang, W. Freude, and J. Leuthold, "Cross-gain modulation-based 2R regenerator using quantum-dot semiconductor optical amplifiers at 160 Gbit/s," *Proc. Conf. ICTON*, Vol. 1, 106–109, TuA1, 2007.
39. Wang, Q., G. Zhu, H. Chen, J. Jaques, J. Leuthold, A. B. Piccirilli, and N. K. Dutta, "Study of all-optical XOR using Mach-Zehnder interferometer and differential scheme," *IEEE Journal of Quantum Electronics*, Vol. 40, No. 6, 703–710, Jun. 2004.
40. Nakahara, T. and R. Takahashi, "Self-stabilizing optical clock pulse-train generator using SOA and saturable absorber for asynchronous optical packet processing," *Optics Express*, Vol. 21, No. 9, 10712–10719, 2013.